Outage Analysis of Wireless-Powered Relaying FSO-RF Systems with Nonlinear Energy Harvesting

Jiliang Zhang[a], Honglin Ran[a], Xiaojun Pan[a], Gaofeng Pan[b,c], Yiyuan Xie[a]

[a]*Key Laboratory of Networks and Cloud Computing Security of Universities in Chongqing, School of Electronic and Information Engineering, Southwest University, Chongqing* 400715*, P.R. China*
[b]*School of Information and Electronics Engineering, Beijing Institute of Technology, Beijing, 100081, P. R. China*
[c]*Computer, Electrical and Mathematical Sciences and Engineering Division, King Abdullah University of Science and Technology (KAUST), Thuwal 23955-6900, Saudi Arabia*

Abstract

In this paper, the outage analysis of a wireless-powered relaying based dual-hop mixed free space optical-radio frequency (FSO-RF) system, which consists of a source (S), a relay (R), a destination (D), and a power beacon (PB), is studied. Specifically, we consider the case where S sends an optical signal to R, R processes the received signal, converts it into a RF signal, and transmits it to D with the energy harvested from PB. Assuming R is with a nonlinear energy harvester, the effects of atmospheric turbulence, two types of detection techniques, pointing error and saturation threshold of the energy harvester on the outage performance are studied. In particular, the closed-form expression for the outage probability is derived. In addition, Monte Carlo simulation results are used to verify the accuracy of the derived expressions.

Keywords: Free space optical-radio frequency (FSO-RF), Gamma-Gamma fading, wireless-powered relaying, outage probability, nonlinear.

1. Introduction

Recently, radio frequency (RF) spectrum scarcity has become the biggest and most concerned issue in the field of wireless communications [1]. The use of additional RF bandwidth allocation in the recent year is no longer a viable solution to meet higher data rate requirements [2]. On the other hand, the free space optical (FSO) communication system has the advantages of license-free spectrum, high bandwidth, and high security [3]. Moreover, it can

also support more users and solve the problems that RF communication systems may encounter in spectrum scarcity [4]. Therefore, the relay-assisted RF-FSO systems can enjoy the joint advantages of RF and FSO techniques to significantly increase data rates and capacity compared to the traditional RF-RF communication systems [5]. In literature, there are several works study the RF-FSO systems [6]-[8]. Ref. [6] studied the outage probability (OP) and ergodic capacity (EC) in an asymmetric dual-hop RF-FSO system under Nakagami-m and M*á*laga (M) fading channel conditions. The trade-off between security and reliability of a multiuser single-input multiple-output (SIMO) mixed RF-FSO system with opportunistic user scheduling schemes was investigated in [7]. Ref. [8] proposed a SIMO wiretap model, and studied the impact of imperfect channel state information (CSI), misalignment, detection technology and relaying schemes on the secrecy outage performance.

On the other hand, the area of energy harvesting (EH) has been widely concerned by academia and industry, as it can effectively solve the problems of limited energy storage capacity, intermittent and scarce environmental energy, and the size and complexity of constrained devices [9], [10]. In [11], the authors analyzed the OP of a wireless-powered relaying (WPR) system using time switching and amplify-and-forward strategies. Assumed the channel experiences Nakagami-m considering both perfect and imperfect CSI scenarios, the outage performance of a decode-and-forward (DF) cooperative network with spatial random WPR was considered in [12]. The authors in [13] studied the relay selection schemes in the presence of imperfect CSI and eavesdropping, and derived an analytical expression for secrecy outage probability (SOP). Considering a multiple-input single-output (MISO) simultaneous wireless information and power transfer downlink system, the analytical expressions for SOP and the average secrecy capacity were derived in the presence of transmit antenna selection and incomplete CSI in [14].

Therefore, it is very interesting and promising to study EH in RF-FSO systems, especially when the relays or other devices are not connected to the electric grid or without any power supply, and they need to harvest energy from the environment to play their roles. However, only a few work in literature invested this issue [15]-[17]. Ref. [15] considered the scenario that the energy and information signals were transmitted to the receiver simultaneously through the FSO link, and presented the closed-form expressions for throughput and OP, and

studied the optimal power allocation strategies under quasi-static and fast fading conditions. Assuming the RF receiver simultaneously collects energy and information from the relay node, the effects of EH on secrecy performance was analyzed in [16]. Considering the scenario that the secondary user (SU) obtained energy from the hybrid SU relays and the primary network under cognitive radio systems, the authors in [17] studied the exact OP, average bit error rate, and EC in a mixed MISO RF-FSO network under Nakagami-m and Málaga (M) fading models.

In this work, we consider a WPR mixed FSO-RF system. Specifically, taking into account the joint effects of atmospheric turbulence, pointing error, detection techniques as well as saturation threshold, the closed-form expression for OP is derived. In addition, as shown in [18] and [19], the nonlinear model is more practical, because the linear energy harvester model may lead to serious mismatches in resource allocation, resulting in significant performance degradation in practical application [18]. Therefore, the nonlinear EH model at WPR is also considered in this system.

2. System and Channel Model

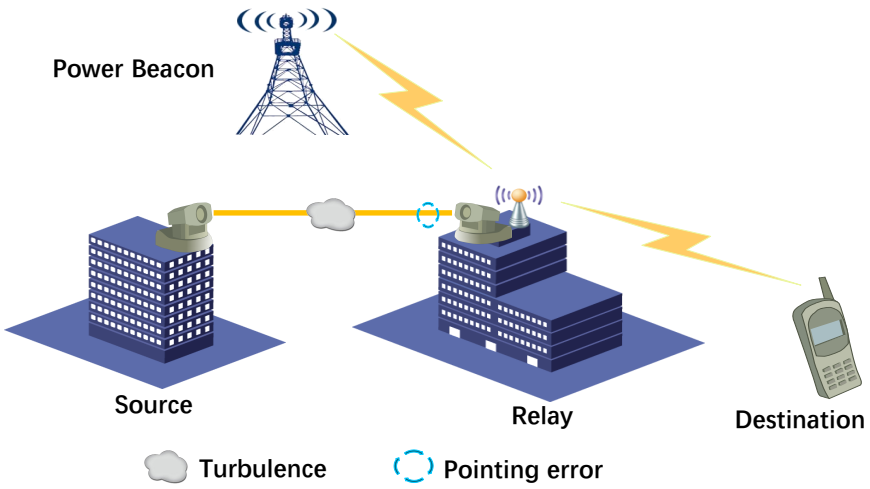

Figure 1: System model.

As shown in Fig. 1, we consider a dual-hop mixed FSO-RF system, which consists of a source (S) node, a relay (R) node, a destination (D) node and a power beacon (PB). It is assumed that S is equipped with a transmission aperture, PB and D are equipped with a

single RF antenna, and R is equipped with both a single RF antenna and a receiving aperture. The whole communication process can be divided into two equal time slots. In the first time slot, S transmits an optical signal to R via FSO channel, which is assumed to experience Gamma-Gamma fading. Then, R decodes the received optical signal and converts it into a RF signal with the optical conversion rate η_1. Simultaneously, R harvests the RF energy from PB with a nonlinear energy harvester. In the second time slot, R consumes all the harvested energy to forward the RF signal to D via the RF channel. It is assumed that all RF channels have identical independent Rayleigh distribution with the channel coefficients denoted as $h_b,\ b \in \{BR, RD\}$. Thus, $|h_b|^2$ has an exponential distribution with the probability density function (PDF) and cumulative distribution function (CDF) denoted as

$$f_{|h_b|^2}(x) = \lambda_b \exp\left(-\lambda_b x\right) \tag{1}$$

and

$$F_{|h_b|^2}(x) = 1 - \exp\left(-\lambda_b x\right) \tag{2}$$

respectively, in which $\lambda_b = \frac{1}{g_b}$ and g_b denotes expectation of channel power gain [13].

In the first time slot, the instantaneous electrical signal-to-noise ratio (SNR) at R can be expressed as

$$\gamma_{SR} = \frac{\eta_1^2 \zeta^2 I^2}{N_0} = \bar{\gamma}_{SR} I^2 \tag{3}$$

where ζ is the photoelectric conversion factor, I is the received optical irradiance, N_0 represents the variance of the additive white Gaussian noise (AWGN), and $\bar{\gamma}_{SR} = \frac{\eta_1^2 \zeta^2}{N_0}$ denotes the average SNR. The PDF of instantaneous SNR, γ_{SR}, is given as [16]

$$f_{\gamma_{SR}}(\gamma) = A \frac{1}{\gamma} G_{1,3}^{3,0}\left[h\alpha\beta \left(\frac{\gamma}{u_r}\right)^{\frac{1}{r}} \middle| \begin{matrix} \xi^2 + 1 \\ \xi^2, \alpha, \beta \end{matrix} \right] \tag{4}$$

where $A = \frac{\xi^2}{r\Gamma(\alpha)\Gamma(\beta)}$, $h = \frac{\xi^2}{\xi^2+1}$, and $\xi = \frac{\omega_e}{2\sigma_s}$ is the ratio between equivalent beam radius and the pointing error displacement standard deviation (jitter) [20]. The notation, r, represents the detection type (i.e., r= 1 represents heterodyne detection (HD) and r= 2 denotes in intensity modulation with direct detection (IM/DD)). α and β are the fading parameters which relates to the atmospheric turbulence conditions [21]. $\Gamma(\cdot)$ is a gamma function defined by (8.310) in [23]. u_r is the average electrical SNR of the FSO link, with $u_1 = E[\gamma_{SR}] = \bar{\gamma}_{SR}$, for HD detection, and $u_2 = \frac{\bar{\gamma}_{SR}\alpha\beta\xi^2(\xi^2+2)}{(\alpha+1)(\beta+1)(\xi^2+1)^2}$, for IM/DD detection. The expression, $G_{p,q}^{m,n}(x\Big|\begin{matrix}a_1,...,a_p\\ b_1,...,b_q\end{matrix})$, is a Meijer G-function defined by (9.301) of [23]. The CDF of γ_{SR} can be expressed as

$$F_{\gamma_{SR}}(\gamma) = B{\cdot}G_{r+1,3r+1}^{3r,1}\left(\rho\gamma\Big|\begin{matrix}1,\kappa_1\\ \kappa_2,0\end{matrix}\right) \tag{5}$$

where

$$B = \frac{\xi^2 r^{\alpha+\beta-2}}{(2\pi)^{r-1}\Gamma(\alpha)\Gamma(\beta)}, \tag{6}$$

$$\rho = \frac{(h\alpha\beta)^r}{\mu_r r^{2r}}, \tag{7}$$

$$\kappa_1 = \triangle(r, \xi^2+1), \tag{8}$$

$$\kappa_2 = \triangle(r, \xi^2), \triangle(r, \alpha), \triangle(r, \beta), \tag{9}$$

and $\triangle(k, a)$ can be defined as

$$\triangle(k, a) = \frac{a}{k}, \frac{a+1}{k}, ..., \frac{a+k-1}{k} \tag{10}$$

which has k terms.

Simultaneously, the PB sends energy signal to R through the RF link and the harvested energy at R can be expressed as

$$E_R = \eta P_B |h_{BR}|^2 T/2 \tag{11}$$

where P_B is the transmission power at PB, T is the block transmission duration and η $(0 \leq \eta \leq 1)$ is the energy conversion efficiency. Since the nonlinear mode is considered, the output power, $P_R = \frac{E_R}{T/2}$, at R can be expressed as [24]

$$P_R = \begin{cases} \eta P_B |h_{BR}|^2 & \text{if } P_B |h_{BR}|^2 \leq \Gamma \\ \eta \Gamma & \text{if } P_B |h_{BR}|^2 > \Gamma \end{cases} \tag{12}$$

where Γ is the saturation threshold of the energy harvester at R.

In the second time slot, the received signal at D is expressed as

$$y_{RD} = \sqrt{P_R} h_{RD} x_R + n_D \tag{13}$$

and the received instantaneous SNR can be denoted as

$$\gamma_{RD} = \frac{P_R |h_{RD}|^2}{N_0} \tag{14}$$

where x_R is the transmission symbol, and n_D is the AWGN with zero mean and a variance of N_0.

3. Outage Performance Analysis

In this section, we will present the derivation of OP. The instantaneous capacity for the S-R and R-D links can be obtained as

$$C_{SR} = \frac{1}{2} \log_2 (1 + \gamma_{SR}) \tag{15}$$

and

$$C_{RD} = \frac{1}{2}\log_2(1+\gamma_{RD}). \tag{16}$$

From the perspective of capacity, the capacity of the whole system will be controlled by the worse hop [25]. Hence, the instantaneous capacity is

$$C_I = \min(C_{SR}, C_{RD}). \tag{17}$$

When C_I is lower than the target threshold C_T (i.e.,$C_I < C_T$), outage occurs. As the two hops are independent of each other, the OP can be expressed as

$$\begin{aligned}
P_{OP} &= Pr\{C_I < C_T\} \\
&= Pr(\min(C_{SR}, C_{RD}) < C_T) \\
&= 1 - Pr(\min(C_{SR}, C_{RD}) \geq C_T) \\
&= 1 - Pr(C_{SR} \geq C_T, C_{RD} \geq C_T) \\
&= 1 - Pr(C_{SR} \geq C_T)Pr(C_{RD} \geq C_T) \\
&= 1 - [1 - Pr(\gamma_{SR} < 2^{2C_T} - 1)]Pr(\gamma_{RD} \geq 2^{2C_T} - 1) \\
&= 1 - [1 - F_{\gamma_{SR}}(\Theta)]Pr(\gamma_{RD} \geq \Theta)
\end{aligned} \tag{18}$$

where $\Theta = 2^{2C_T} - 1$.

Making use of (12) and (14), the term, $Pr(\gamma_{RD} \geq \Theta)$, in (18) can be re-expressed as

$$Pr(\gamma_{RD} \geq \Theta) = M_1 + M_2 \tag{19}$$

where

$$M_1 = Pr(|h_{BR}|^2 z \geq D, |h_{BR}|^2 \leq E) \tag{20}$$

and

$$M_2 = Pr(z \geq F, |h_{BR}|^2 > E) \tag{21}$$

in which $D = \frac{N_0\Theta}{\eta P_B}$, $E = \frac{\Gamma}{P_B}$, $F = \frac{N_0\Theta}{\eta\Gamma}$, and $z = |h_{RD}|^2$.

Because $|h_{BR}|^2$ is a non-negative random variable and D is a positive value. Let the inequality $|h_{BR}|^2 z \geq D$ holds in (20), z must be positive (i.e., $z > 0$). The PDF of z can be expressed as

$$f_z(z) = \lambda_{RD} \exp\left(-\lambda_{RD} z\right). \tag{22}$$

Therefore, M_1 can be rewritten as

$$\begin{aligned}
M_1 &= Pr(|h_{BR}|^2 \geq \frac{D}{z}, |h_{BR}|^2 \leq E, z > 0) \\
&= Pr\left(\frac{D}{z} \leq |h_{BR}|^2 \leq E, z \geq \frac{D}{E}\right) \\
&= \int_{\frac{D}{E}}^{\infty} \int_{\frac{D}{z}}^{E} f_{|h_{BR}|^2}(x) f_z(z) dx dz \\
&= \int_{\frac{D}{E}}^{\infty} \left[F_{|h_{BR}|^2}(E) - F_{|h_{BR}|^2}(\frac{D}{z})\right] f_z(z) dz \\
&= I_1 - I_2.
\end{aligned} \tag{23}$$

Substituting (1) and (22) into (23), one can obtain

$$\begin{aligned} I_1 &= \int_{\frac{D}{E}}^{\infty} \exp\left(- \frac{\lambda_{BR} D}{z} \right) f_z(z) dz \\ &= \lambda_{RD} \times \int_{\frac{D}{E}}^{\infty} \exp\left(- \lambda_{RD} z - \frac{\lambda_{BR} D}{z} \right) dz \\ &= \lambda_{RD} \times \left[\int_{0}^{\infty} \exp\left(- \lambda_{RD} z - \frac{\lambda_{BR} D}{z} \right) dz - \int_{0}^{\frac{D}{E}} \exp\left(- \lambda_{RD} z - \frac{\lambda_{BR} D}{z} \right) dz \right] \end{aligned} \tag{24}$$

and

$$\begin{aligned} I_2 &= \int_{\frac{D}{E}}^{\infty} \exp(-\lambda_{BR} E) f_z(z) dz \\ &= \exp\left(- \lambda_{BR} E - \frac{\lambda_{RD} D}{E} \right). \end{aligned} \tag{25}$$

Using the approximation in [22] and (3.471.9) in [23], I_1 can be rewritten as

$$I_1 \approx \lambda_{RD} \times 2 \left(\frac{\lambda_{BR} D}{\lambda_{RD}} \right)^{\frac{1}{2}} K_1(2\sqrt{\lambda_{BR} \lambda_{RD} D}) \left[1 - \left(1 - \exp(-\lambda_{RD} \frac{D}{E}) \right) \right]. \tag{26}$$

Next, M_2 can be rewritten as

$$M_2 = Pr(z \geq F) Pr(|h_{BR}|^2 > E) \tag{27}$$

where

$$\begin{aligned} Pr(z \geq F) &= \int_{F}^{\infty} f_z(z) dz \\ &= \exp\left(-\lambda_{RD} F\right) \end{aligned} \tag{28}$$

and

$$Pr(|h_{BR}|^2 > E) = \exp\left(-\lambda_{BR} E\right). \tag{29}$$

Finally, substituting (5), (23), and (27) into (18), the OP can be obtained as

$$P_{OP} = 1 - \left[1 - B{\cdot}G_{r+1,3r+1}^{3r,1}\left(\rho\Theta\middle|\begin{matrix}1,\kappa_1\\ \kappa_2,0\end{matrix}\right)\right] \times \left[\lambda_{RD} \times 2\left(\frac{\lambda_{BR}D}{\lambda_{RD}}\right)^{\frac{1}{2}} K_1(2\sqrt{\lambda_{BR}\lambda_{RD}D}) \times \exp(-\lambda_{RD}\frac{D}{E})\right] - \exp\left(-\lambda_{BR}E - \frac{\lambda_{RD}D}{E}\right) + \exp(-\lambda_{RD}F - \lambda_{BR}E)\Bigg]. \tag{30}$$

4. Numerical Results and Discussions

In this section, we present the numerical results and discuss the effects of different parameters on the outage performance. Unless otherwise explicitly specified, the parameters of these results are set as: $\eta = 0.9$, $\eta_1 = 1$, $\zeta = 1$, $N_0 = 1$, $g_{BR} = 1\ dB$, $\alpha = 2.902$, $\beta = 2.510$ (weak turbulence), $\alpha = 2.296$, $\beta = 1.822$ (moderate turbulence), and $\alpha = 2.064$, $\beta = 1.342$ (strong turbulence).

Figs. 2-4 show the OP versus $\bar{\gamma}_{SR}$ under different conditions. It can be observed that as $\bar{\gamma}_{SR}$ increases, the outage performance is improved. However, increasing $\bar{\gamma}_{SR}$ does not always lead to better outage performance. This is because the system capacity is limited by the dual hop of the system, and when $\bar{\gamma}_{SR}$ is bigger than a certain value (i.e., $\bar{\gamma}_{SR} > 40$ dB, as shown in Fig. 2), the system performance is dominated by the second hop, which is unchanged. We also observe that the HD technique (r=1) can result in better outage performance than the IM/DD technique (r=2). This is because the SNR obtained with the HD scheme is higher than that with the IM/DD scheme. In addition, the outage performance for a higher value of (α,β) outperforms that with a lower value of (α,β), as the atmospheric turbulence only affects the SNR at R. It's further observed that the OP with a higher ξ is superior to that with a lower one. This is due to the fact that a larger value of ξ has a higher pointing accuracy.

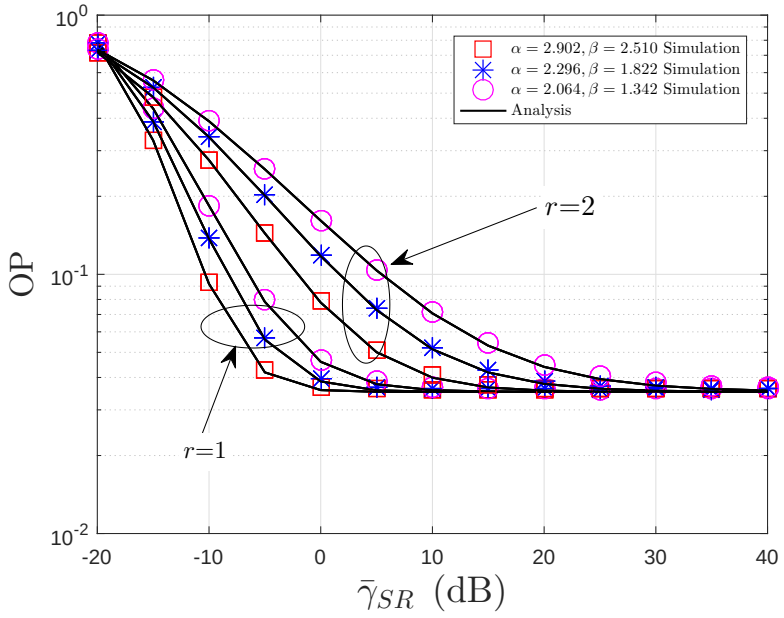

Figure 2: OP versus $\bar{\gamma}_{SR}$ with ξ= 6.7, g_{RD}= 1 dB, P_B/N_0= 10 dB, Γ/P_B= -5.4 dB, and C_{th}=0.01 bits/s/Hz.

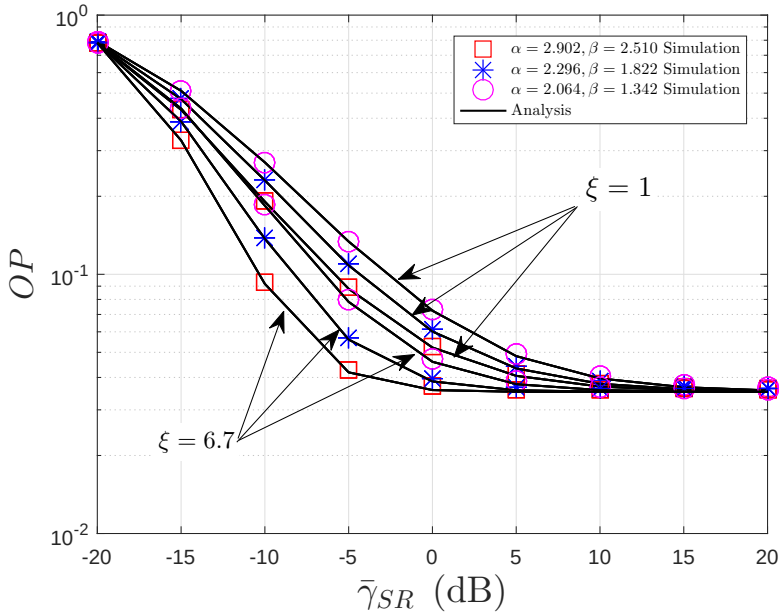

Figure 3: OP versus $\bar{\gamma}_{SR}$ with r= 1, g_{RD}= 1 dB, P_B/N_0= 10 dB, Γ/P_B= -5.4 dB, and C_{th}=0.01 bits/s/Hz.

Fig. 5 shows the OP versus g_{RD} under different turbulence conditions and pointing errors. It can be observed that when $g_{RD} < 40$ dB, the outage performance can be improved with the increasing of g_{RD}. While $g_{RD} > 40$ dB, increasing g_{RD} has little effect on the outage performance. This is due to the fact that when $g_{RD} > 40$ dB, the first hop is dominated,

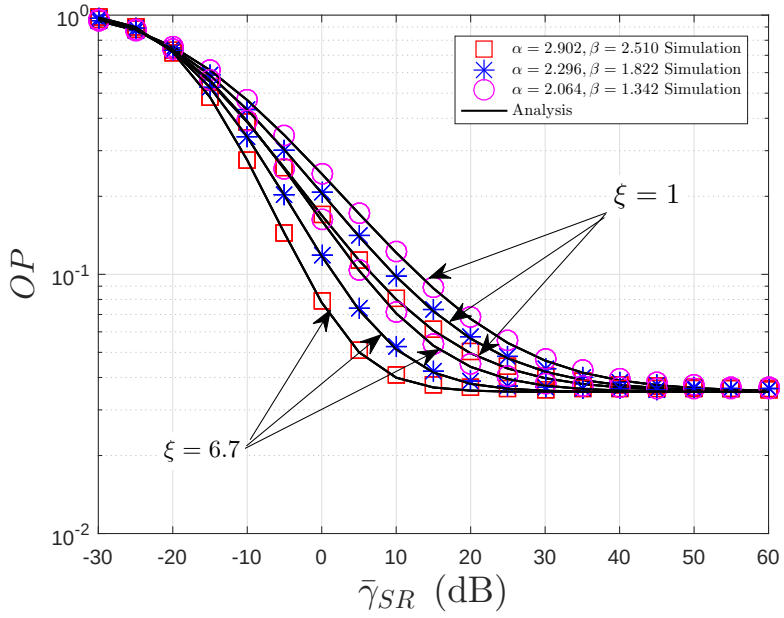

Figure 4: OP versus $\bar{\gamma}_{SR}$ with r= 2, g_{RD}= 1 dB, P_B/N_0= 10 dB, Γ/P_B= -5.4 dB, and C_{th}=0.01 bits/s/Hz.

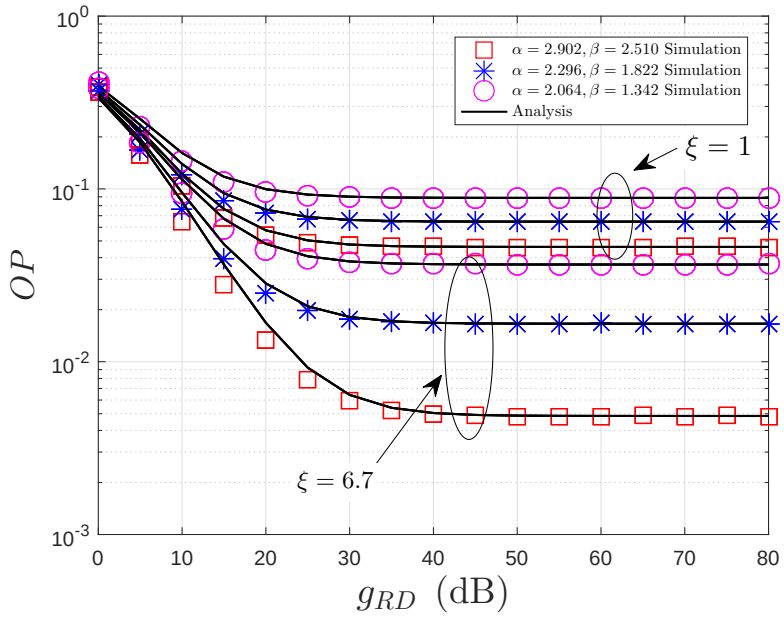

Figure 5: OP versus g_{RD} with r= 1, $\bar{\gamma}_{SR}$= 5 dB, P_B/N_0= 1 dB, Γ/P_B= -4 dB, and C_{th}=0.08 bits/s/Hz.

which is not improved.

As depicted in Fig. 6, the OP versus Γ is presented under different turbulence conditions and pointing errors. It is easy to observe that the outage performance can be properly improved with higher saturation threshold when Γ/P_B < -10 dB. This is because the

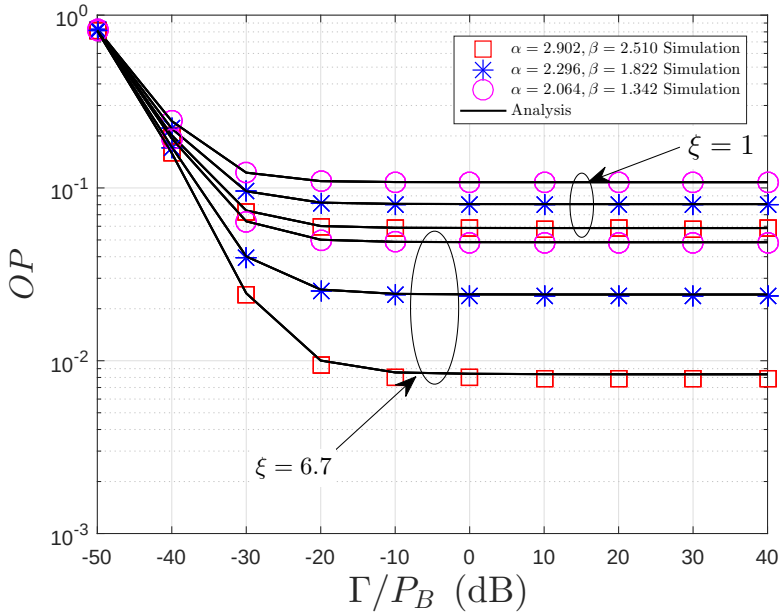

Figure 6: OP versus Γ/P_B with r= 1, $\bar{\gamma}_{SR}$= 5 dB, P_B/N_0= 5 dB, g_{RD}= 35 dB, and C_{th}=0.1 bits/s/Hz.

battery with higher storage capability can ensure more harvested energy for information transmission. When $\Gamma/P_B >$ -10 dB, it is observed that the outage performance will remain unchanged. The reason is that increasing Γ will only improve the capability of the battery, but the energy harvested from PB is not increased, as the transmission power at PB remains unchanged.

Finally, it is observed that the simulation results are very consistent with the analytical results in all the figures, which confirms the analytical expression derived.

5. Conclusion

In this paper, the outage performance of a mixed FSO-RF system with WPR is analyzed. Considering the combined effects of atmospheric turbulence, pointing error, detection techniques, and the saturation threshold, the closed-form expressions for OP have been derived. Monte Carlo simulation verifies that the HD method has better outage performance than the IM/DD method. And the OP with a higher ξ is better than that with a lower one. Furthermore, when the saturation threshold exceeds a certain value, the outage performance remains unchanged.

6. References

[1] Ansari IS, Abdallah MM, Alouini M, and Qaraqe KA. Outage performance analysis of underlay cognitive RF and FSO wireless channels. in Proc. IWOW, Funchal, Portugal, Sep. 2014, pp. 6-10.

[2] Haykin S. Cognitive radio: Brain-empowered wireless communications. IEEE J. Sel. Areas Commun. 2005; 23(2): 201-220.

[3] Balti E, Guizani M, Hamdaoui B, and Khalfi B. Aggregate hardware impairments over mixed RF/FSO relaying systems with outdated CSI. IEEE Trans. Commun. 2018; 66(3): 1110-1123.

[4] Lee E, Park J, Han D, and Yoon G. Performance analysis of the asymmetric dual-hop relay transmission with mixed RF/FSO links. IEEE Photon. Technol. Lett. 2011; 23(21): 1642-1644.

[5] Al-Eryani YF, Salhab AM, Zummo SA, and Alouini MS. Two-way multiuser mixed RF/FSO relaying: Performance analysis and power allocation. IEEE/OSA J. Opt. Commun. Netw. 2018; 10(4): 396-408.

[6] Palliyembil V, Vellakudiyan J, Muthuchidamdaranathan P, and Tsiftsis TA. Capacity and outage probability analysis of asymmetric dual-hop RF-FSO communication systems. IET Commun. 2018; 12(16): 1979-1983.

[7] El-Malek AHA, Salhab AM, Zummo SA, and Alouini MS. ecurity-reliability trade-off analysis for multiuser SIMO mixed RF/FSO relay networks with opportunistic user scheduling. IEEE Trans. Wireless Commun. 2016; 15(9): 5904-5918.

[8] Lei H, Luo H, Park KH, Ren Z, Pan G, and Alouini MS. Secrecy outage analysis of mixed RF-FSO systems with channel imperfection. IEEE Photon. J. 2018; 10(3): 1-13.

[9] Sudevalayam S, Kulkarni P. Energy harvesting sensor nodes: Survey and implications. IEEE Commun. Surv. Tutor. 2011; 13(3): 443-461.

[10] Chen J, Yang L, Wang W, Yang HC, Liu Y, Hasna MO, and Alouini MS. A novel energy harvesting scheme for mixed FSO-RF relaying systems. IEEE Trans. Veh. Technol. 2019; 68(8): 8259-8263.

[11] Dong Y, Hossain MJ, and Cheng J. Performance of wireless powered amplify and forward relaying over nakagami-m fading channels with nonlinear energy harvester. IEEE Commun. Lett. 2016; 20(4): 672-675.

[12] Ye J, Lei H, Liu Y, Pan G, da Costa DB, Ni Q, and Ding Z. Cooperative communications with wireless energy harvesting over nakagami-m fading channels. IEEE Trans. Commun. 2017; 65(12): 5149-5164.

[13] Zhang J, Pan G, and Xie Y. Secrecy analysis of wireless-powered multi-antenna relaying system with nonlinear energy harvesters and imperfect CSI. IEEE Trans. Green Commun. Netw. 2018; 2(2): 460-470.

[14] Pan G, Lei H, Deng Y, Fan L, Yang J, Chen Y, and Ding Z. On secrecy performance of MISO SWIPT systems with TAS and imperfect CSI. IEEE Trans. Commun. 2016; 64(9): 3831-3843.

[15] Makki B, Svensson T, Buisman K, Perez J, and Alouini MS. Wireless energy and information transmission in FSO and RF-FSO links. IEEE Wireless Commun. Lett. 2018; 7(1): 90-93.

[16] Lei H, Dai Z, Park KH, Lei W, Pan G, and Alouini MS. Secrecy outage analysis of mixed RF-FSO downlink SWIPT systems. IEEE Trans. Commun. 2018; 66(12): 6384-6395.

[17] El-Malek AHA, Aboulhassan MA, Salhab AM, and Zummo SA. Performance analysis and power optimization for spectrum-sharing mixed RF/FSO relay networks with energy harvesting. IEEE Photon. J. 2019; 11(2): 1-17.

[18] Boshkovska E, Ng DWK, Zlatanov N, Koelpin A, and Schober R. Robust resource allocation for MIMO wireless powered communication networks based on a non-linear EH model. IEEE Trans. Commun. 2017; 65(5): 1984-1999.

[19] Boshkovska E, Ng DWK, Zlatanov N, and Schober R. Practical non-linear energy harvesting model and resource allocation for SWIPT systems. IEEE Commun. Lett. 2015; 19(12): 2082-2085.

[20] Ansari IS, Yilmaz F, and Alouini MS. Performance analysis of free-space optical links over M*álaga (M)* turbulence channels with pointing errors. IEEE Trans. Wireless Commun. 2016; 15(1): 91-102.

[21] Zedini E, Soury H, and Alouini MS. On the performance analysis of dual-hop mixed FSO/RF systems. IEEE Trans. Wireless Commun. 2016; 15(5): 3679-3689.

[22] Yan M, Chen Q, Lei X, Duong TQ and Fan P. Outage probability of switch and stay combining in two-way amplify-and-forward relay networks. in IEEE Wireless Commun. Lett. 2012; 1(4): 296-299.

[23] Gradshteyn I, Ryzhik IM. Table of Integrals, Series and Products, 7th Ed. San Diego: Academic Press; 2007.

[24] Zhang J, Pan G, and Xie Y. Secrecy outage performance for wireless-powered relaying systems with nonlinear energy harvesters. Front. Inform. Technol. Electron. Eng. 2017; 18(2): 246-252.

[25] Ai Y, Mathur A, Cheffena M, Bhatnagar MR, and Lei H. Physical layer security of hybrid satellite-FSO cooperative systems. IEEE Photon. J. 2019; 11(1): 1-14.